

1 **Two years online measurement of fine particulate nitrate in western**
2 **Yangtze River Delta: Influences of thermodynamics and N₂O₅ hydrolysis**

3 Peng Sun¹, Wei Nie^{1,2,*}, Xuguang Chi^{1,2}, Yuning Xie¹, Xin Huang^{1,2}, Zheng Xu^{1,2}, Ximeng Qi^{1,2}, ,
4 Zhengning Xu¹, Lei Wang¹, Tianyi Wang¹, Qi Zhang³, and Aijun Ding^{1,2,*}

5

6 ¹Joint International Research Laboratory of Atmospheric and Earth System Science s, and School of
7 Atmospheric Sciences, Nanjing University, Nanjing, 210023, China

8 ²Jiangsu Provincial Collaborative Innovation Center of Climate Change, Nanjing, 210023, China

9 ³Department of Environmental Toxicology, University of California, Davis, CA 95616, USA

10 Correspondence: Wei Nie (niewei@nju.edu.cn) and Aijun Ding (dingaj@nju.edu.cn)

11 **Abstract.**

12 Particulate nitrate contributes a large fraction of secondary aerosols. Despite
13 understanding of its important role in regional air quality and global climate, long-term
14 continuous measurements are rather limited in China. In this study, we conducted online
15 measurement of PM_{2.5} nitrate for two years from March 2014 to February 2016 using
16 the Monitor for Aerosols and Gases in ambient Air (MARGA) in the western Yangtze
17 River Delta (YRD), eastern China, and investigate the main factors that influenced its
18 temporal variations and formation pathways. Compared to other sites in China, an
19 overall high concentration of particulate nitrate was observed with a mean value of 15.8
20 $\mu\text{g m}^{-3}$ (0.5 to 92.6 $\mu\text{g m}^{-3}$). Nitrate on average accounted for 32% of the total mass of
21 water-soluble ions and the proportion increased with PM loading, indicating that nitrate
22 is a major driver of haze pollution episodes in this region. Sufficient ammonia drove
23 most nitrate into the particle phase in the form of ammonium nitrate. A typical seasonal
24 cycle of nitrate was observed with the concentrations in winter on average two times
25 higher than those in summer mainly due to different meteorological conditions. In
26 summer, the diurnal variation of particulate nitrate was determined by the
27 thermodynamic equilibrium, resulting in a much lower concentration during daytime
28 despite of a considerable photochemical production. Air masses from polluted YRD

29 and biomass burning region contributed to the high nitrate concentration during summer.
30 In winter, particulate nitrate didn't reveal an evident diurnal variation. Regional
31 transport from northern China played an important role in enhancing nitrate
32 concentration. Eighteen nitrate episodes were selected to understand the processes that
33 drive the formation of high concentration of nitrate. Rapid nitrate formation was
34 observed during the pre-episode (the day before nitrate episode day) nights, and
35 dominated the increase of total water-soluble ions. Calculated nitrate from N_2O_5
36 hydrolysis was highly correlated to and accounted for 80 percent of the observed nitrate,
37 suggesting that N_2O_5 hydrolysis was a major contributor to the nitrate episodes. Our
38 results suggested that rapid formation of nitrate could be a main cause for extreme
39 aerosol pollution events in YRD during winter, and illustrated the urgent needs to
40 control the NO_x emission.

41 **1. Introduction**

42 Particulate nitrate (NO_3^-), as a major aerosol component in the atmosphere, reduces
43 atmospheric visibility (Charlson and Heintzenberg, 1995), influences human health,
44 alters radiative forcing and hence influences regional even global climate (IPCC, 2013).
45 Compared to the sulfate, nitrate has a larger scattering albedo under low RH conditions
46 that cause a stronger influence on visibility (Lei and Wuebbles, 2013). High
47 concentration of particulate nitrate had been demonstrated to be one of the major
48 reasons for the frequent occurrence of haze episodes in China (Wang and Zhang, 2009;
49 Wen et al., 2015; Wang et al., 2017). In recent decades, the Chinese government started
50 to control emissions of air pollutants with special effort on the SO_2 reduction. This
51 resulted in a remarkable decrease of ambient SO_2 and sulfate concentrations after 2006
52 (van der A et al., 2017; Wang et al., 2017). However, particulate nitrate, as well as its
53 proportion in PM, showed increasing trends due to the strong emission of nitrogen
54 oxides (NO_x) (Lei and Wuebbles, 2013; Yang et al., 2017).

55 Particulate nitrate can be formed from multiple pathways. Gas phase reaction of
56 NO_2 and OH radical is one major pathway to form nitric acid (HNO_3) (Calvert and

57 Stockwell, 1983), which subsequently reacts with ammonia (NH_3) to produce
58 ammonium nitrate (NH_4NO_3). As typical photochemical processes, these reactions
59 dominate daytime nitrate formation, and have been widely investigated in both field
60 and modelling studies (Sharma et al., 2007; Petetin et al., 2016). Heterogeneous uptake
61 of the photochemical formed nitric acid by alkali compounds, e.g. dust and sea salt
62 particles, is also a considerable pathway to form nitrate in some regions (Bian et al.,
63 2014). During nighttime, the hydrolysis of dinitrogen pentoxide (N_2O_5) is believed to
64 be the dominate pathway to form particulate nitrate. N_2O_5 is an important reactive
65 nitrogen species in the polluted troposphere (Brown and Dube., 2007; Osthoff et al.,
66 2006; Li et al., 2017; Brown et al., 2003; Brown and Stutz, 2012; Wang et al., 2016d;
67 Wang et al., 2017b) and accumulates via the reversible reaction between NO_2 and NO_3
68 radical produced from the reaction of NO_2 with O_3 . Due to the rapid photolysis of NO_3
69 radical, [the contribution of \$\text{N}_2\text{O}_5\$ hydrolysis to nitrate concentration during daytime of](#)
70 [sunny day is usually small](#). While during nighttime, N_2O_5 concentration can be up to
71 ppb level, and form nitric acid by reaction with water vapor, or particulate nitrate
72 directly by heterogeneous hydrolysis on the wet surface (Wang et al., 2017a; Wen et al.,
73 2018; Thornton et al., 2003). In China, the pollution episodes with high nitrate
74 concentrations mostly occurred in winter, during which the photochemical production
75 of nitrate should be overall weak. N_2O_5 hydrolysis thus has the potential to be the
76 crucial contributor, however there is still a lack of observational evidences.

77 Collecting particulate matter on a filter with subsequent ion chromatography
78 analysis in laboratories is the conventional method to measure the concentration of
79 particulate nitrate. The [un-denuded](#) filter pack system, which is most-widely used, can
80 suffer from both positive artifacts by absorbing gas-phase nitric acid, and negative
81 artifacts by the evaporation of ammonium nitrate (Nie et al., 2010; Pathak and Wu,
82 2009; Wang et al., 2010). A denuder system can minimize these sampling artifacts by
83 adding denuders to remove the interfering gases and back-up filters to collect the
84 evaporated vapors (John et al., 1988). However, the operation of such a denuder system

85 is [extremely](#) labor intensive and thus not widely used. In addition, the poor time-
86 resolution of filter-based measurement can limit our understanding on the formation
87 and chemical evolution of the particulate nitrate. To overcome these shortcomings,
88 several continuous and semi-continuous techniques have been developed based on an
89 online [denuded-IC](#) system (e.g. the ambient ion monitor (AIM), the gas and aerosol
90 collector ion chromatography (GAC-IC), the particle-into-liquid sample ion
91 chromatography (PILS-IC) and MARGA), as well as mass spectrometry (e.g. AMS).
92 Pathak et al. (2011) applied an AIM instrument in Beijing and Shanghai for one month
93 and found that the heterogeneous hydrolysis of N_2O_5 contributed 50%~100% of the
94 nighttime nitrate formation. Xue et al. (2013) deployed a PILS-IC system in Hong Kong
95 for less than a month and showed a more active nitrate formation during PM episode
96 than normal days. Wen et al. (2015) used a MARGA instrument in Yucheng, North
97 China during summer and emphasized the important roles of O_3 and NH_3 on nitrate
98 formation. Yang et al. (2017) carried out field observation with ACSM in Beijing for
99 half a month and pointed out the importance of aerosol nitrate in haze formation.
100 However, despite of an increasing number of studies using online techniques,
101 continuous measurements with more than one-year period are still very limited.

102 The Yangtze River Delta (YRD) located in the eastern China, with megacities
103 including Shanghai, Nanjing and Suzhou etc., has suffered from heavy particulate
104 matter pollution and photochemical pollution (Ding et al., 2013bc; Wang et al., 2016bc;
105 Wang et al., 2016a). Previous studies indicated an important role of nitrate in the
106 pollution episodes (Hua et al., 2015; Du et al., 2011; Yang et al., 2017). For example,
107 [Zhang et al. \(2015a\)](#) carried out an observation with ACSM in urban Nanjing during
108 summer and autumn, and found nitrate and organic aerosols dominated the PM_{10}
109 composition. Shi et al. (2014) used MARGA instrument in Shanghai for months and
110 found an increasing contribution of nitrate to PM_{10} mass during pollution periods.
111 Wang et al. (2016b) reported temporal variation and transport of $PM_{2.5}$ water soluble
112 ions, including nitrate, in an urban site in Shanghai based on three-year continuous

113 measurement using MARGA. However, detailed investigation of the possible
114 mechanisms governing nitrate behaviors during haze pollution is still rare.

115 In this study, we present a 2-year continuous measurement of particulate nitrate
116 using MARGA at a rural site in Nanjing, a megacity in the western YRD region, with
117 the target to get a comprehensive understanding of particulate nitrate behaviors and
118 investigate the processes affecting nitrate in haze episodes. We first conducted general
119 statistical analysis of particulate nitrate and characterized seasonal variation and diurnal
120 pattern. A thermodynamic model was then applied to investigate the gas-particle
121 partition of nitrate. The influence of air masses was also investigated by conducting
122 backward Lagrangian dispersion modelling. Finally, we selected eighteen nitrate
123 episodes and investigated the main processes influencing their evolution.

124 **2. Methodology**

125 2.1. Sample site and instrumentation

126 The SORPES station (118°57'E, 32°07'N) was located on the top of a small hill (40 m
127 above sea level) in the Xianlin campus of Nanjing University located in the outskirts of
128 Nanjing, China. The station is an ideal receptor of air masses from the YRD with little
129 influence of local emissions and urban pollution from Nanjing. Detailed description can
130 be found in previous studies (Ding et al., 2013c; Ding et al., 2016a).

131 The measurement was conducted from March 2014 to Feb 2016. Hourly
132 concentrations of water soluble gases of HCl, HNO₃, HONO, SO₂ and NH₃, and water-
133 soluble ions in PM_{2.5}, including Cl⁻, NO₃⁻, SO₄²⁻, NH₄⁺, Na⁺, K⁺, Ca²⁺, and Mg²⁺, were
134 measured with a Monitor for Aerosols and Gases in ambient Air (MARGA, designed
135 and manufactured by Applikon Analytical B.V., the Netherlands) employed in
136 connection with a Thermo PM_{2.5} cyclone inlet. The sampling system was comprised of
137 two parts: A Wet Rotating Denuder for gases and a Steam Jet Aerosol Collector for
138 aerosols, working at an air flow of 1 m³ h⁻¹ (ten Brink et al., 2007; Rumsey et al., 2014).
139 After each hour's collection, the samples were analyzed using ion chromatography. The
140 instrument was calibrated on an hourly basis using internal standard liquid (bromide

141 lithium), ensuring a stable and reliable ion chromatograph. Concentrations of all aerosol
142 ions and gases have a precision of $0.001\mu\text{g m}^{-3}$ (Xie et al., 2015). The $\text{PM}_{2.5}$ ion dataset
143 from the MARGA provided more than 15000 hourly samples over the 24 months of
144 measurements considering points where NO_3^- , NH_4^+ and SO_4^{2-} were all available. Trace
145 gases (i.e., O_3 , SO_2 , NO_x , NO) and $\text{PM}_{2.5}$ mass concentrations were also measured at
146 SORPES (Ding et al., 2013c; Nie et al., 2015; Ding et al., 2016a), together with
147 meteorological data including wind speed/direction, temperature, and relative humidity.

148 2.2. Thermodynamic constants and ISORROPIA II

149 Formation of ammonium nitrate involves an equilibrium reaction between the gas phase
150 NH_3 and HNO_3 , and particle phase NH_4NO_3 . The gas-to-particle partitioning is
151 temperature dependent, and the equilibrium constant can be calculated as follows (units
152 $\text{mol}^2\text{kg}^{-2}\text{atm}^{-2}$) (Sun et al., 2011; Seinfeld and Pandis, 2006):

$$153 \quad K=k_{298} \exp(a(298/T-1) +b[1+\ln(298/T)-298/T]) \quad (1)$$

$$154 \quad K_{298}=3.5\times 10^{16}(\text{atm}^{-2}), a=75.11, b=-13.5. \quad (2)$$

155 ISORROPIA II (available at <http://isorro피아.eas.gatech.edu/>) is a thermodynamic
156 model used commonly in inorganic aerosol research (Fountoukis and Nenes, 2007). To
157 analyze gas-into-particulate pathway for nitrate formation, HNO_3 was modeled with
158 ISORROPIA II run in forward model iteratively (Pusede et al., 2016; Fountoukis and
159 Nenes, 2007). ISORROPIA II was initialized as $[\text{NO}_3^-+\text{HNO}_3]_{\text{total}} = [\text{NO}_3^-]_{\text{aerosol}}$.
160 Calculated $\text{HNO}_3(\text{g})$ was added back to $[\text{NO}_3^-+\text{HNO}_3]$, while we always use
161 $[\text{NH}_4^+_{\text{aerosol}}+\text{NH}_3(\text{g})]$ as input total ammonium. ISORROPIA II was solved iteratively
162 until output NO_3^- changed by $< 2\%$ by mass. The phase state was set as metastable. We
163 assume that gases and aerosol are in equilibrium, that aerosols are homogeneous and
164 internally mixed, and that unaccounted-for factors do not influence the thermodynamics
165 of system (Vayenas et al., 2005).

166 2.3. Lagrangian Dispersion Modeling

167 To help understand the influence of air masses, backward Lagrangian particulate
168 dispersion modeling (LPDM) was carried out based on a method developed and

169 evaluated by Ding (Ding et al., 2013a). The LPDM was conducted using the Hybrid
170 Single-Particulate Lagrangian Integrated Trajectory model developed in the Air
171 Resource Laboratory (ARL) of the National Oceanic and Atmospheric Administration
172 using the ARL format Global Data Assimilation System data. The model calculates the
173 position of particulates by mean wind and a turbulence transport component after they
174 are released at the source point for a backward simulation. For each hour, 3000
175 particulates were released at 100 m altitude over the site and were traced backward for
176 a 3-day period. The hourly position of each particulate was calculated using a 3-D
177 particulate, i.e., horizontal and vertical, method. The residence time at 100 m altitude,
178 i.e., foot-print “retroplume”, which represents the distribution of the surface probability
179 or residence time of the simulated air mass, was used to understand the contribution
180 from potential source regions (Ding et al., 2013ac; Shen et al., 2018).

181 2.4. Steady-state predictions

182 Based on their short lifetimes, the concentrations of the NO_3 radical and N_2O_5 can be
183 predicted by steady-state calculations due to lack of measurement data (Osthoff et al.,
184 2006). The formation and loss of N_2O_5 associated with a series of chemical reactions
185 are listed in Table 1. For the heterogeneous processes, we used 0.004 and 0.03 as the
186 uptake coefficients of the NO_3 radical and N_2O_5 (γNO_3 and $\gamma\text{N}_2\text{O}_5$), respectively
187 (Aldener et al., 2006; Wen et al., 2015; Knopf et al., 2011; Brown et al., 2006). Due to
188 the lack of measurement during 2014 - 2016, the VOCs data used here was the average
189 of nighttime value that measured at SORPES station during the wintertime of 2017.
190 The corresponding rate constant can be found in Master Chemical Mechanism (MCM
191 version 3.1, <http://mcm.leeds.ac.uk/MCM/>). The uncertainty that caused by the limited
192 VOCs measurements and the variation of N_2O_5 uptake coefficient were estimated and
193 discussed in the supplement.

194 3. Results and discussion

195 3.1. Overall results

196 A MARGA was deployed to continuously measure the eight water-soluble ions (WSI)

197 of PM_{2.5} and several gas-phase species from March 2014 to February 2016 with the
198 time resolution of 1-hour. Nitrate (NO₃⁻), sulfate (SO₄²⁻) and ammonium (NH₄⁺) were
199 the major components with the two-year averaged concentrations of 15.8 (±13.4), 15.3
200 (±10.6) and 10.4 (±7.6) μg m⁻³, respectively. In the present study, we focused on nitrate,
201 and discussed the temporal variation and its association with physicochemical
202 processes. The concentration of PM_{2.5} nitrate changed largely from 0.5 to 92.6 μg m⁻³
203 during the measurement period, and accounted for 3% to 58% of total WSI (=45.7 +
204 30μg m⁻³). The highest hourly nitrate concentration occurred on December 23, 2015
205 together with high concentrations of sulfate (65.5 μg m⁻³), and ammonium (56.8 μg m⁻³).
206 Heavy haze episode like this occurred at our site frequently during winter. To
207 understand the influence of wind on nitrate concentration, the wind rose plot is given
208 in Fig. S2. The prevailing winds at the SORPES station were from northeast and east
209 during the two-year observation period. Particulate nitrate tended to accumulate or
210 formed under stagnant condition of low wind speed. The wind from west and east can
211 lead to a higher nitrate concentration and also other aerosol components (Ding et al.,
212 2013bc; Shen et al., 2018), which may be associated with air masses from biomass
213 burning region and the city clusters of YRD.

214 To get an overall picture of nitrate distribution in developed region of costal China,
215 we reviewed results from available nitrate measurements in three most polluted regions
216 of North China Plain (NCP), YRD and Pearl River Delta (PRD), and summarized their
217 concentration, sampling sites and measurement techniques in Fig.1. The corresponding
218 data and references are listed in table S1. Measurements in summer and winter were
219 separated due to the large seasonal difference of particulate nitrate. Despite that these
220 measurements were from various measurement techniques, the results still can give us
221 some insights about the differences in spatial and temporal scales. First, particulate
222 nitrate generally showed the highest concentration in NCP and followed by YRD and
223 PRD. This was in consistence with the spatial distribution of NO₂ – a major gas
224 precursor of nitrate. Second, evident seasonal variations can be observed at all three

225 regions with much higher concentrations in winter. Third, an overall increase of
226 particulate nitrate was implied in NCP and YRD in the past decade, especially that
227 during summertime. Nevertheless, particulate nitrate in PRD revealed an overall
228 decreasing trend. It should be noted that the dataset cited in Fig. 1 were obtained from
229 different sites with different techniques. Trends inferred from these dataset could suffer
230 from considerable uncertainty. Compared to these previous studies, the nitrate
231 concentration during summertime at SORPES station was lower than that in NCP, but
232 higher than that in YRD and PRD cities. In terms of wintertime, nitrate concentration
233 at SORPES station was slightly lower than that in NCP, comparable with that in YRD,
234 and higher than that in PRD.

235 Fig. 2 illustrates the occurrence frequency of the loading of particle matter in
236 different concentration ranges, and the changes of nitrate proportion along with the PM
237 loading. Noting that the PM loading here was indicated by the mass of total WSI. The
238 highest frequency of WSI concentrations occurred in a range of 20-40 $\mu\text{g m}^{-3}$, and
239 gradually decreased with the increasing of concentration. Heavy PM pollution with
240 WSI concentrations higher than 100 $\mu\text{g m}^{-3}$ occurred during more than 5% of the time
241 during this study. The contribution of nitrate to total WSI increased with the PM loading,
242 ranging from ~25% with WSI concentration lower than 20 $\mu\text{g m}^{-3}$ to ~40% when WSI
243 was higher than 140 $\mu\text{g m}^{-3}$. These results suggested that nitrate was a major driver of
244 haze episodes with high PM peaks in this region.

245 Fig. 3a shows the scatter plot of particulate nitrate and total WSI. The correlation
246 coefficient was 0.92 and nitrate accounted for 32% of the total WSI. Air temperature
247 greatly affected the contribution of nitrate to total WSI. Its proportion can be up to 58%
248 at in the temperature range of 0 °C to 5 °C and only 3% at the temperature higher than
249 30 °C, indicating an important role of thermodynamic equilibrium in nitrate
250 concentration. We further investigated the neutralization extent of sulfate and nitrate by
251 ammonium (Fig. 3b). Ammonium was overall enough to neutralize both sulfate and
252 nitrate, suggesting that the particulate nitrate mostly existed as ammonium nitrate at

253 SORPES station. This is different from the ammonia poor regions, where the uptake of
254 HNO_3 to dust/sea salt particles was found to be important to $\text{PM}_{2.5}$ nitrate (Griffith et
255 al., 2015). Seasonal difference can be observed for the molar ratio of ammonium to the
256 sum of sulfate and nitrate. In spring and early summer, a fraction of the particulate
257 nitrate is present as $\text{Ca}(\text{NO}_3)_2$ and KNO_3 , which could explain the data points below the
258 regression line in Fig. 3b. In winter, considerable ammonium is existed as NH_4Cl (Hu
259 et al., 2017), resulting in the data points above the regression line.

260 3.2. Characteristics of fine particular nitrate in different seasons.

261 3.2.1. Seasonal pattern and its main causes

262 Fig. 4 shows the composite seasonal pattern of NO_x , $\text{PM}_{2.5}$ nitrate, sulfate and the
263 molar-based ratio of nitrate to sulfate during the 2-year period at SORPES station. The
264 seasonal variations of other related species and nitrate-to- $\text{PM}_{2.5}$ -ratio are shown in Table
265 S2. Similar to the previous studies (Griffith et al., 2015), a typical seasonal variation
266 was observed for particulate nitrate (and its ratio to sulfate, i.e. $\text{NO}_3^-/\text{SO}_4^{2-}$), with a
267 maximum value of $23.7 \mu\text{g m}^{-3}$ (140%) in January, and a minimum of $8.4 \mu\text{g m}^{-3}$ (66%)
268 in August and September. Particulate sulfate exhibits a relatively less pronounced
269 seasonal pattern with a small peak in June. The low value of particulate nitrate during
270 summer can be generally explained by the higher temperature, higher and unstable
271 boundary layer and relative clean air masses induced by summer monsoon (Ding et al.,
272 2013c) despite of the increased photochemical formation. In opposite, the high values
273 during winter were generally due to the lower temperature, lower and stable boundary
274 layer and relative stronger continental outflow from the North China where
275 anthropogenic emission was relatively high due to heating in winter (Ding et al., 2013c).
276 Different chemical processes that affects nitrate concentrations between summer and
277 winter will be discussed later. NO_x , the major precursor, tracked the changes of
278 particulate nitrate, except for that during February and June. In addition, a secondary
279 peak of particulate nitrate can be observed during June, which can be explained as the
280 influence from agricultural burning in eastern China (Ding et al., 2013bc; Xie et al.,

281 2015; Shen et al., 2018). The concentrations of Potassium, a biomass burning tracer in
282 this region (Ding et al., 2013b; Xie et al., 2015), clearly showed a consistent peak (Fig.
283 S3) with both particulate nitrate and sulfate, as well as the discrepancy of NO_x and
284 nitrate concentrations (Ding et al., 2013b; Xie et al., 2015; Nie et al., 2015) shown in
285 Fig. 4. While in February, the nitrate concentration didn't show concurrent decrease in
286 NO_x during the Chinese Spring Festival (Ding et al., 2013c). [The observations might](#)
287 [suggest that particulate nitrate is influenced by regional transport but not the local](#)
288 [emissions in February.](#)

289 3.2.2. Diurnal cycles during summer and winter

290 In Fig. 5, we show the averaged diurnal variations of particulate nitrate, nitrogen
291 dioxide, nitric acid, equilibrium constant (K), air temperature and RH during summer
292 and winter during the two years. Nitric acid was calculated by ISORROPIA II. In
293 summer (Fig. 5a), the fine particulate nitrate showed a typical diurnal cycle that the
294 maximum concentration occurred at 7:00 with the average concentration of 16.5 $\mu\text{g m}^{-3}$
295 and minimum value at 14:00 (7.2 $\mu\text{g m}^{-3}$). This summertime diurnal pattern of nitrate
296 is very similar with the findings in Shandong (Wen et al., 2015) and New York (Sun et
297 al., 2011). However, it is quite different from the findings in Hong Kong (Griffith et al.,
298 2015), where nitrate concentration peaks in the daytime in summer. Ambient
299 temperature and the development of boundary layer are the major drivers to the
300 observed diurnal variation of particulate nitrate, [and high temperature and high](#)
301 [boundary layer during daytime lead to evaporation and dilution of the particulate nitrate](#)
302 (Zhang et al., 2015a; Ding et al., 2016). Nitric acid, which accounted for 20% of the
303 total nitrate [$\text{NO}_3^- + \text{HNO}_3$], revealed its high concentration (around 2 ppb) in the
304 noontime (12:00-15:00). NO₂, the precursor of nitrate, showed a peak concentration of
305 18.2 ppb at 21:00, and remained at a high level during the whole night. [The](#) Equilibrium
306 constant, K , was calculated to understand the influence of gas-to-particulate partitioning
307 on the observed diurnal variation of particulate nitrate (Sun et al., 2011). As showed in
308 Fig. 5a, [K showed the same diurnal pattern as particulate nitrate,](#) suggesting the

309 thermodynamic is the major factor influencing the diurnal variation of particle nitrate
310 during summer.

311 In winter, the diurnal variation is small with a moderate peak at around 10:00 AM.
312 Compared to that in summer, K showed similar diurnal variation, but not correlated to
313 particulate nitrate, indicating factors other than the control of temperature. The
314 observed peak at late morning was probably due to downward mixing from the residual
315 layer where particulate nitrate was formed aloft during the night and brought to the
316 surface after sunrise following the breakup of the boundary layer (Baasandorj et al.,
317 2017; Young et al., 2016; Pusede et al., 2016). Direct vertical observations are needed
318 to further investigate this issue.

319 To further investigate factors influencing the nitrate behaviors other than
320 thermodynamics, ISORROPIA II was used to simulate the diurnal variation of nitrate.
321 Hourly concentrations of all species (both gas and aerosol phase species) at 00:00 were
322 used as the initial value of each specific day. Hourly data of temperature and relative
323 humidity were used as the input data to constrain the model. The ISORROPIA II model
324 was set as forward mode and metastable phase state. The calculated diurnal variations
325 are shown in Fig. 6 together with the observed results.

326 The differences between the calculation and the observation could be attributed to:
327 (1) the development of boundary layer, (2) the dry deposition of nitric acid, and (3)
328 chemical processes, which has not been considered yet in the model. As shown in Fig.
329 6a, the overall diurnal pattern of nitrate in summer is well captured by the model except
330 for 3 periods. The differences after midnight are likely caused by the effect of boundary
331 layer height and some chemical processes. Faster increase of model nitrate after 18:00
332 was attributed to lack of dry deposition of nitric acid in the model. During noontime the
333 observed nitrate concentration was expected to be lower than the calculated value
334 because of the development of boundary layer and stronger dry deposition of nitric acid
335 associated with stronger turbulence mixing, which were neglected in the model.
336 However, in contrast, the observation was considerably higher than the calculated value.

337 It indicates a strong production of nitrate via photochemical processes in summer.
338 Fig.6c shows that the difference between calculated and observed nitrate concentration
339 was in good correlation with the [product](#) of NO₂ and solar radiation, a proxy for the
340 production rate of nitric acid (Zhang et al., 2005; Young et al., 2016), further suggesting
341 that photo-oxidation of NO₂ is an important source of nitrate during summer, even
342 though the thermodynamic equilibrium is the dominate factor controlling the diurnal
343 cycle. Wen et al. (2018) also demonstrated that photochemical production of nitric acid
344 is a major contributor to daytime nitrate increase during summer in North China Plain.
345 [In winter, the influence of thermodynamics on diurnal cycle is small since the relatively](#)
346 [low temperature throughout the day.](#) The peaks in the morning may be caused by the
347 mixing down of a residual layer enriched of nitrate as mentioned above, while the
348 decline during the afternoon are supposed to be the result of dilution associated with
349 the boundary layer development.

350 3.2.3 Influence of air masses transport

351 Meteorological processes play a key role in air masses long-range transport and local
352 accumulation (Ding et al., 2013ac; Zhang et al., 2016; Ding et al, 2016b). In order to
353 investigate the influence of air masses transport on nitrate concentrations, Lagrangian
354 dispersion modeling was conducted for the sampling days with the top and bottom 25%
355 nitrate concentration in summer and winter, respectively (Ding et al., 2013a). Fig. 7
356 shows the retroplumes, i.e. footprint at an altitude of 100 m, of the selected days during
357 summer and winter, respectively. In summer, high concentrations of nitrate tended to
358 [be associated](#) with the air masses from west of Nanjing (mostly Anhui province) and
359 Yangtze River Delta (Suzhou-Shanghai city clusters and North Zhejiang province) (Fig.
360 7a). YRD is a high NO_x emission region (Fig. 1), air masses from which could bring
361 high concentration of NO_x to enhance the nitrate concentration at SORPES station.
362 Biomass burning is the possible cause of the high nitrate loading with air mass from the
363 west of Nanjing (Fig. S4). In winter, regional transport from northern China played an
364 important role in enhancing nitrate concentrations. As shown in Fig. 8c, a large part of

365 air masses for the highest 25% sampling days was from North China Plain, which has
366 the strongest NO_x emission in China (Fig. 1). It should be noted here that the longer
367 lifetime of particulate nitrate during winter might be the main cause to promote the
368 contribution of regional transport to the observed nitrate at SORPES. In contrast, the
369 lowest 25% sampling days during winter tended to be accompanied with the air mass
370 from Nanjing local and marine areas.

371 3.3. Contribution of N₂O₅ hydrolysis to nitrate episodes

372 Similar to findings from previous studies (Zhang et al., 2015c), nitrate was found to
373 increase significantly during this study and become the largest contributor of PM_{2.5}
374 during the haze episodes (Fig. 2). Generally, these pollution episodes mainly occurred
375 in winter (Fig. 3a and Fig. 4), during which the photochemical production of nitric acid
376 should be weak. N₂O₅ hydrolysis was thus proposed to be a potential important
377 formation pathway. Here we investigated the nitrate episodes in detail and discussed
378 their relationship to the N₂O₅ hydrolysis during the nights before.

379 In Fig. 8, we show a typical case of nitrate episodes from 30 November to 2
380 December, 2015. Fast nitrate formation was observed, which was likely caused by
381 hydrolysis of N₂O₅. Nitrate increased significantly from 20.3 μg m⁻³ at 18:00 of 30
382 November to 63 μg m⁻³ at 6:00 of 1 December, 2015. The ratio of nitrate to PM_{2.5} also
383 exhibited a large increase from 25% at 18:00 to 38% at 06:00. In contrast, other PM_{2.5}
384 components, e.g. sulfate and black carbon, showed only slight increases. High
385 concentration of NO₂, considerable level of O₃ and extremely low concentration of NO
386 provided a favorable condition towards forming NO₃ and N₂O₅ (Brown et al., 2003).
387 The meteorological conditions during these 12 hours were stable with low wind speed
388 and high relative humidity, which, combined with the relatively high concentration of
389 PM, would promote the hydrolysis of N₂O₅ (Riemer, 2003).

390 N₂O₅ concentrations were calculated by using the steady-state approximation
391 (Osthoff et al., 2006; Wang et al., 2014; Wen et al., 2015), and the result was shown in
392 Fig. 8. The calculated N₂O₅ exhibited a much higher concentration during the night of

393 30 November compared to the days before and after. Particulate nitrate formed from
394 N_2O_5 hydrolysis was then computed during the 12-hour period. Nitrate concentration
395 at 18:00 of 30 November, 2015 ($20 \mu\text{g m}^{-3}$) was selected as the initial value, and $31 \mu\text{g}$
396 m^{-3} of particulate nitrate was produced in the following 12 hours, suggesting that
397 approximate 80% of increased particulate nitrate can be attributed to the hydrolysis of
398 N_2O_5 in this case.

399 To further understand the contribution of N_2O_5 hydrolysis, sampling days with
400 daily-averaged nitrate concentration exceeding the mean plus twice the standard
401 deviation were selected as the nitrate episode days. In total, 18 episode-days were
402 selected during the 2-year measurement, with 16 days in winter and the other 2 days in
403 biomass burning season. In Fig. 9, we presented the averaged diurnal pattern of
404 particulate nitrate and its related parameters on the 18 selected episode and pre-episode
405 days. For the episode days, particulate nitrate revealed a similar diurnal pattern as that
406 of the whole winter (Fig. 5). Nitrate maintained a high concentration during the whole
407 day with a small peak around 10:00 in the morning. However, for the pre-episode days,
408 a clear build-up of nitrate can be observed, especially during the nighttime from 17:00
409 of the pre-episode days to 1:00 of the episode days (as marked in Fig. 9). The average
410 increment of ammonium nitrate exceeded $24 \mu\text{g m}^{-3}$ during this 9-hour period of the
411 pre-episode nighttime. The total WIS also increased during this period, which was
412 mostly attributed to ammonium nitrate (almost 90%) and resulted in an evident increase
413 of the ratio of nitrate to total WSI. Compared to nitrate, black carbon, a tracer of primary
414 emissions, showed little change during the pre-episode day. The retroplume showed in
415 Fig. S5 suggested that the air masses arrived at the SORPES station on the pre-episode
416 and episode days were almost the same. These results suggest that secondary formation
417 other than accumulation was the major contributor to the observed increase of
418 particulate nitrate.

419 Since the observed nitrate formation mostly occurred during the nighttime of pre-
420 episode days when the photochemical production of nitric acid would be largely

421 suppressed, N_2O_5 hydrolysis is thus believed to be the major contributor. As showed in
422 Fig. 9, compared to those during episode days, NO_2 concentration was comparable with
423 the average concentrations of 28 ppb, the but O_3 concentration was higher during pre-
424 episode days. This resulted in a higher production rate of N_2O_5 proxy (PNO_3) in pre-
425 episode days, and favored formation of nitrate from the hydrolysis of N_2O_5 . We further
426 calculated the contribution of N_2O_5 hydrolysis to nitrate formation during the periods
427 from 17:00 to 23:00 of each pre-episode day (excluding 2 windy days). A good
428 correlation ($R=0.8$) was observed between the calculated nitrate and observed nitrate
429 (Fig. 10), with the slope of 0.77, indicating the observed nitrate formation during nitrate
430 episodes were significantly attributed to the hydrolysis of N_2O_5 . It should be noted that
431 this calculation suffered from considerable uncertainties due to the variability of actual
432 VOCs concentrations and N_2O_5 uptake coefficient. The detailed uncertainty calculation
433 is discussed in the supplement (Fig. S1).

434 4. Summary and Conclusion

435 Online measurements of fine particulate nitrate along with trace gases and $\text{PM}_{2.5}$ mass
436 concentrations were conducted for two years from March 2014 to February 2016 using
437 a MARGA at SORPES station, a rural receptor site in the Yangtze River Delta, eastern
438 China. Hourly nitrate concentration varied from $0.5 \mu\text{g m}^{-3}$ to $92.6 \mu\text{g m}^{-3}$, with an
439 averaged value of $15.8 \mu\text{g m}^{-3}$, which was generally higher than the measurement at the
440 sites in YRD and PRD, but lower than that at the sites in North China Plain. The
441 contribution of nitrate to total WSI increased from 25% with WSI concentration lower
442 than $20 \mu\text{g m}^{-3}$, to 40% when WSI was higher than $140 \mu\text{g m}^{-3}$, suggesting a major
443 driver of nitrate to the aerosol pollution in YRD. NH_3 is enough to neutralize the acidic
444 compounds of aerosol, and ammonium nitrate was thus the predominate form of the
445 observed particulate nitrate. A clear seasonal variation of nitrate was observed with
446 peak value in January and December and lowest value in August and September.
447 Biomass burning plumes contributed to the nitrate concentration evidently and resulted
448 in a secondary peak during June. In summer, thermodynamic equilibrium was the major

449 factor influencing the diurnal variation of nitrate, and resulted in a much lower
450 concentration at noontime. Nevertheless, the observed nitrate at noontime was
451 considerably higher than the value predicted by the ISORROPIA II model, indicating a
452 strong production of nitrate by the photo-oxidation of NO_2 . Air masses from YRD and
453 the biomass burning region were associated with the high nitrate concentrations during
454 summer. In winter, the diurnal variation of nitrate was weak. Regional transport from
455 the North China Plain contributed largely to the observed high nitrate concentrations.

456 Nitrate episodes, defined as daily-averaged concentration exceeding the mean
457 value plus twice the standard deviation, were further investigated to understand the
458 chemical processes towards forming particulate nitrate and their contribution to the
459 pollution episodes. A clear build-up of nitrate can be observed during the pre-episode
460 night, which dominated the increase of total WSI. N_2O_5 hydrolysis was demonstrated
461 to contribute 80% of the observed nitrate formation, suggesting its critical role in an
462 aerosol pollution episode. In view of the significant emission of NO , which is the main
463 sink of N_2O_5 during night, stronger production of N_2O_5 is expected at the upper
464 boundary layer, e.g. residual layer, and this residual layer N_2O_5 will contribute to the
465 nitrate formation in the entire boundary layer. In summary, our study provides evidence
466 that particulate nitrate especially that formed from N_2O_5 hydrolysis is a crucial
467 contributor to the aerosol pollution episodes in eastern China.

468 *Data availability.* The GDAS data used in the HYSPLIT calculation can be acquired
469 from <ftp://arlftp.arlhq.noaa.gov/pub/archives/gdas1>. Measurement data at SORPES,
470 including aerosol data and relevant trace gases as well as meteorological data, are
471 available upon request from the corresponding author before the SORPES database is
472 opened publicly.

473 *Acknowledgements.* The research was supported by National Key Research &
474 Development Program of China (2016YFC0200500) and National Science Foundation

475 of China (41725020, 91544231, 91644218, 41422504, 91744311, 41675145).

476 **References**

- 477 Aldener, M., Brown, S. S., Stark, H., Williams, E. J., Lerner, B. M., Kuster, W. C., Goldan, P. D., Quinn,
478 P. K., Bates, T. S., Fehsenfeld, F. C., and Ravishankara, A. R.: Reactivity and loss mechanisms of
479 NO₃ and N₂O₅ in a polluted marine environment: Results from in situ measurements during New
480 England Air Quality Study 2002, *J Geophys Res-Atmos*, 111, 2006.
- 481 Baasandorj, M., Hoch, S. W., Bares, R., Lin, J. C., Brown, S. S., Millet, D. B., Martin, R., Kelly, K.,
482 Zarzana, K. J., Whiteman, C. D., Dube, W. P., Tonnesen, G., Jaramillo, I. C., and Sohl, J.: Coupling
483 between Chemical and Meteorological Processes under Persistent Cold-Air Pool Conditions:
484 Evolution of Wintertime PM_{2.5} Pollution Events and N₂O₅ Observations in Utah's Salt Lake Valley,
485 *Environ Sci Technol*, 51, 5941-5950, 10.1021/acs.est.6b06603, 2017.
- 486 Bian, Q., Huang, X. H. H., and Yu, J. Z.: One-year observations of size distribution characteristics of
487 major aerosol constituents at a coastal receptor site in Hong Kong – Part 1: Inorganic ions
488 and oxalate, *Atmospheric Chemistry and Physics*, 14, 9013-9027, 10.5194/acp-14-9013-2014, 2014.
- 489 Brown, S. S., Stark, H., Ryerson, T. B., Williams, E. J., Nicks, D. K., Trainer, M., Fehsenfeld, F. C., and
490 Ravishankara, A. R.: Nitrogen oxides in the nocturnal boundary layer: Simultaneous in situ
491 measurements of NO₃, N₂O₅, NO₂, NO, and O₃, *J Geophys Res-Atmos*, 108, 2003.
- 492 Brown, S. S., Ryerson, T. B., Wollny, A. G., Brock, C. A., Peltier, R., Sullivan, A. P., Weber, R. J., Dube,
493 W. P., Trainer, M., Meagher, J. F., Fehsenfeld, F. C., and Ravishankara, A. R.: Variability in nocturnal
494 nitrogen oxide processing and its role in regional air quality, *Science*, 311, 67-70, 2006.
- 495 Brown, S. S., and W.P.Dube.: High resolution vertical distributions of NO₃ and N₂O₅ through the
496 nocturnal boundary layer, *Atmospheric Chemistry and Physics*, 7, 139-149, 2007.
- 497 Brown, S. S., and Stutz, J.: Nighttime radical observations and chemistry, *Chem Soc Rev*, 41, 6405-6447,
498 2012.
- 499 Brown, S. S., Dube, W. P., Tham, Y. J., Zha, Q. Z., Xue, L. K., Poon, S., Wang, Z., Blake, D. R., Tsui,
500 W., Parrish, D. D., and Wang, T.: Nighttime chemistry at a high altitude site above Hong Kong, *J*
501 *Geophys Res-Atmos*, 121, 2457-2475, 10.1002/2015JD024566, 2016.
- 502 Calvert, J. G., and Stockwell, W. R.: Acidic generation in the troposphere by gas phase chemistry,
503 *Environ. Sci. Technol.*, 17, 428-443, 1983.
- 504 Cao, J.-J., Shen, Z.-X., Chow, J. C., Watson, J. G., Lee, S.-C., Tie, X.-X., Ho, K.-F., Wang, G.-H., and
505 Han, Y.-M.: Winter and Summer PM_{2.5} Chemical Compositions in Fourteen Chinese Cities, *Journal*
506 *of the Air & Waste Management Association*, 62, 1214-1226, 10.1080/10962247.2012.701193,
507 2012.
- 508 Charlson, R., and Heintzenberg, J.: Aerosol Forcing of Climate Environmental Sciences Research Report,
509 1995.

510 Ding, A., Wang, T., and Fu, C.: Transport characteristics and origins of carbon monoxide and ozone in
511 Hong Kong, South China, *Journal of Geophysical Research: Atmospheres*, 118, 9475-9488,
512 10.1002/jgrd.50714, 2013a.

513 Ding, A. J., Fu, C. B., Yang, X. Q., Sun, J. N., Petäjä, T., Kerminen, V. M., Wang, T., Xie, Y., Herrmann,
514 E., Zheng, L. F., Nie, W., Liu, Q., Wei, X. L., and Kulmala, M.: Intense atmospheric pollution
515 modifies weather: a case of mixed biomass burning with fossil fuel combustion pollution in eastern
516 China, *Atmospheric Chemistry and Physics*, 13, 10545-10554, 10.5194/acp-13-10545-2013, 2013b.

517 Ding, A. J., Fu, C. B., Yang, X. Q., Sun, J. N., Zheng, L. F., Xie, Y. N., Herrmann, E., Nie, W., Petäjä, T.,
518 Kerminen, V. M., and Kulmala, M.: Ozone and fine particle in the western Yangtze River Delta: an
519 overview of 1 yr data at the SORPES station, *Atmospheric Chemistry and Physics*, 13, 5813-5830,
520 10.5194/acp-13-5813-2013, 2013c.

521 Ding, A.J., Nie, W., Huang, X., Chi, X., Sun, J., Kerminen, V.-M., Xu, Z., Guo, W., Petäjä, T., Yang, X.,
522 Kulmala, M., and Fu, C.: Long-term observation of air pollution-weather/climate interactions at the
523 SORPES station: a review and outlook, *Front. Environ. Sci. & Eng.*, 10, 5, 15, 2016a.

524 Ding, A.J., Huang, X., Nie, W., Sun, J.N., Kerminen, V.-M., Petaja, T., Su, H., Cheng, Y.F., Yang, X.-Q.,
525 Wang, M.H., Chi, X.G., Wang, J.P., Virkkula, A., Guo, W.D., Yuan, J., Wang, S.Y., Zhang, R.J., Wu,
526 Y.F., Song, Y., Zhu, T., Zilitinkevich, S., Kulmala, M., and Fu, C.B.: Enhanced haze pollution by
527 black carbon in megacities in China, *Geophys. Res. Lett.*, 43, 6, 2873-2879, 2016b.

528 Du, H., Kong, L., Cheng, T., Chen, J., Du, J., Li, L., Xia, X., Leng, C., and Huang, G.: Insights into
529 summertime haze pollution events over Shanghai based on online water-soluble ionic composition
530 of aerosols, *Atmospheric Environment*, 45, 5131-5137, 10.1016/j.atmosenv.2011.06.027, 2011.

531 Fountoukis, C., and Nenes, A.: ISORROPIA II: a computationally efficient thermodynamic equilibrium
532 model for $K^+-Ca^{2+}-Mg^{2+}-NH_4^+-Na^+-SO_4^{2-}-NO_3^- -Cl^- -H_2O$ aerosols, *Atmospheric Chemistry
533 and Physics*, 7, 4639-4659, 2007.

534 Gao, X. M., Yang, L. X., Cheng, S. H., Gao, R., Zhou, Y., Xue, L. K., Shou, Y. P., Wang, J., Wang, X. F.,
535 Nie, W., Xu, P. J., and Wang, W. X.: Semi-continuous measurement of water-soluble ions in PM_{2.5}
536 in Jinan, China: Temporal variations and source apportionments, *Atmospheric Environment*, 45,
537 6048-6056, 2011.

538 Griffith, S. M., Huang, X. H. H., Louie, P. K. K., and Yu, J. Z.: Characterizing the thermodynamic and
539 chemical composition factors controlling PM_{2.5} nitrate: Insights gained from two years of online
540 measurements in Hong Kong, *Atmospheric Environment*, 122, 864-875,
541 10.1016/j.atmosenv.2015.02.009, 2015.

542 He, L.-Y., Huang, X.-F., Xue, L., Hu, M., Lin, Y., Zheng, J., Zhang, R., and Zhang, Y.-H.: Submicron
543 aerosol analysis and organic source apportionment in an urban atmosphere in Pearl River Delta of
544 China using high-resolution aerosol mass spectrometry, *Journal of Geophysical Research*, 116,
545 10.1029/2010jd014566, 2011.

546 Hu, W., Hu, M., Hu, W.-W., Zheng, J., Chen, C., Wu, Y., and Guo, S.: Seasonal variations in high time-

547 resolved chemical compositions, sources, and evolution of atmospheric submicron aerosols in the
548 megacity Beijing, *Atmospheric Chemistry and Physics*, 17, 9979-10000, 10.5194/acp-17-9979-
549 2017, 2017.

550 Hua, Y., Cheng, Z., Wang, S., Jiang, J., Chen, D., Cai, S., Fu, X., Fu, Q., Chen, C., Xu, B., and Yu, J.:
551 Characteristics and source apportionment of PM_{2.5} during a fall heavy haze episode in the Yangtze
552 River Delta of China, *Atmospheric Environment*, 123, 380-391, 10.1016/j.atmosenv.2015.03.046,
553 2015.

554 John, W., Wall, S. M., and Ondo, J. L.: A New Method for Nitric-Acid and Nitrate Aerosol Measurement
555 Using the Dichotomous Sampler, *Atmospheric Environment*, 22, 1627-1635, 1988.

556 Knopf, D. A., Forrester, S. M., and Slade, J. H.: Heterogeneous oxidation kinetics of organic biomass
557 burning aerosol surrogates by O₃, NO₂, N₂O₅, and NO₃, *Phys Chem Chem Phys*, 13, 21050-
558 21062, 2011

559 Lei, H., and Wuebbles, D. J.: Chemical competition in nitrate and sulfate formations and its effect on air
560 quality, *Atmospheric Environment*, 80, 472-477, 10.1016/j.atmosenv.2013.08.036, 2013.

561 Li, H., Zhang, Q., Zhang, Q., Chen, C., Wang, L., Wei, Z., Zhou, S., Parworth, C., Zheng, B., Canonaco,
562 F., Prévôt, A. S. H., Chen, P., Zhang, H., Wallington, T. J., and He, K.: Wintertime aerosol chemistry
563 and haze evolution in an extremely polluted city of the North China Plain: significant contribution
564 from coal and biomass combustion, *Atmospheric Chemistry and Physics*, 17, 4751-4768,
565 10.5194/acp-17-4751-2017, 2017.

566 Nie, W., Wang, T., Gao, X., Pathak, R. K., Wang, X., Gao, R., Zhang, Q., Yang, L., and Wang, W.:
567 Comparison among filter-based, impactor-based and continuous techniques for measuring
568 atmospheric fine sulfate and nitrate, *Atmospheric Environment*, 44, 4396-4403,
569 10.1016/j.atmosenv.2010.07.047, 2010.

570 Nie, W., Ding, A. J., Xie, Y. N., Xu, Z., Mao, H., Kerminen, V. M., Zheng, L. F., Qi, X. M., Huang, X.,
571 Yang, X. Q., Sun, J. N., Herrmann, E., Petäjä, T., Kulmala, M., and Fu, C. B.: Influence of biomass
572 burning plumes on HONO chemistry in eastern China, *Atmospheric Chemistry and Physics*, 15,
573 1147-1159, 10.5194/acp-15-1147-2015, 2015.

574 Osthoff, H. D., Sommariva, R., Baynard, T., Pettersson, A., Williams, E. J., Lerner, B. M., Roberts, J. M.,
575 Stark, H., Goldan, P. D., Kuster, W. C., Bates, T. S., Coffman, D., Ravishankara, A. R., and Brown,
576 S. S.: Observation of daytime N₂O₅ in the marine boundary layer during New England Air Quality
577 Study-Intercontinental Transport and Chemical Transformation 2004, *Journal of Geophysical*
578 *Research: Atmospheres*, 111, n/a-n/a, 10.1029/2006jd007593, 2006.

579 Pathak, R. K., and W.S.Wu: Summertime PM_{2.5} ionic species in four major cities of China; nitrate
580 formation in an ammonia-deficient atmosphere, *Atmospheric Chemistry and Physics*, 9, 1711-1722,
581 2009.

582 Pathak, R. K., Wang, T., and Wu, W. S.: Nighttime enhancement of PM_{2.5} nitrate in ammonia-poor
583 atmospheric conditions in Beijing and Shanghai: Plausible contributions of heterogeneous

584 hydrolysis of N₂O₅ and HNO₃ partitioning, *Atmospheric Environment*, 45, 1183-1191,
585 10.1016/j.atmosenv.2010.09.003, 2011.

586 Petetin, H., Sciare, J., Bressi, M., Gros, V., Rosso, A., Sanchez, O., Sarda-Estève, R., Petit, J.-E., and
587 Beekmann, M.: Assessing the ammonium nitrate formation regime in the Paris megacity and its
588 representation in the CHIMERE model, *Atmospheric Chemistry and Physics*, 16, 10419-10440,
589 10.5194/acp-16-10419-2016, 2016.

590 Pusede, S. E., Duffey, K. C., Shusterman, A. A., Saleh, A., Laughner, J. L., Wooldridge, P. J., Zhang, Q.,
591 Parworth, C. L., Kim, H., Capps, S. L., Valin, L. C., Cappa, C. D., Fried, A., Walega, J., Nowak, J.
592 B., Weinheimer, A. J., Hoff, R. M., Berkoff, T. A., Beyersdorf, A. J., Olson, J., Crawford, J. H., and
593 Cohen, R. C.: On the effectiveness of nitrogen oxide reductions as a control over ammonium nitrate
594 aerosol, *Atmospheric Chemistry and Physics*, 16, 2575-2596, 10.5194/acp-16-2575-2016, 2016.

595 Riemer, N.: Impact of the heterogeneous hydrolysis of N₂O₅ on chemistry and nitrate aerosol formation
596 in the lower troposphere under photochemical conditions, *Journal of Geophysical Research*, 108,
597 10.1029/2002jd002436, 2003.

598 Rumsey, I. C., Cowen, K. A., Walker, J. T., Kelly, T. J., Hanft, E. A., Mishoe, K., Rogers, C., Proost, R.,
599 Beachley, G. M., Lear, G., Frelink, T., and Otjes, R. P.: An assessment of the performance of the
600 Monitor for Aerosols and Gases in ambient air (MARGA): a semi-continuous method for soluble
601 compounds, *Atmospheric Chemistry and Physics*, 14, 5639-5658, 10.5194/acp-14-5639-2014, 2014.

602 Seinfeld, J. H., and Pandis, S. N.: *Atmospheric Chemistry and Physics: From Air Pollution to Climate*
603 *Change*, John Wiley & Sons, New York, 2nd edition, 1232 pp., 13: 978-0-471-72018-8 2006.

604 Sharma, M., Kishore, S., Tripathi, S. N., and Behera, S. N.: Role of atmospheric ammonia in the
605 formation of inorganic secondary particulate matter: A study at Kanpur, India, *Journal of*
606 *Atmospheric Chemistry*, 58, 1-17, 10.1007/s10874-007-9074-x, 2007.

607 Shen, Y., Virkkula, A., Ding, A., Wang, J., Chi, X., Nie W., Qi, X., Huang, X., Liu Q., Zheng, L., Xu, Z.,
608 Petaja, T., Aalto, P.P., Fu, C. and Kulmala, M.: Aerosol optical properties at SORPES in Nanjing,
609 East China, *Atmos. Chem. Phys.*, 18, 5265-5292, 2018.

610 Shi, Y., Chen, J., Hu, D., Wang, L., Yang, X., and Wang, X.: Airborne submicron particulate (PM₁)
611 pollution in Shanghai, China: chemical variability, formation/dissociation of associated semi-
612 volatile components and the impacts on visibility, *The Science of the total environment*, 473-474,
613 199-206, 10.1016/j.scitotenv.2013.12.024, 2014.

614 Sun, Y. L., Zhang, Q., Schwab, J. J., Demerjian, K. L., Chen, W. N., Bae, M. S., Hung, H. M., Hogrefe,
615 O., Frank, B., Rattigan, O. V., and Lin, Y. C.: Characterization of the sources and processes of
616 organic and inorganic aerosols in New York city with a high-resolution time-of-flight aerosol mass
617 spectrometer, *Atmospheric Chemistry and Physics*, 11, 1581-1602, 10.5194/acp-11-1581-2011,
618 2011.

619 ten Brink, H., Otjes, R., Jongejan, P., and Slanina, S.: An instrument for semi-continuous monitoring of
620 the size-distribution of nitrate, ammonium, sulphate and chloride in aerosol, *Atmospheric*

621 Environment, 41, 2768-2779, 10.1016/j.atmosenv.2006.11.041, 2007.

622 Thornton, J. A., Braban, C. F., and Abbatt, J. P. D.: N₂O₅ hydrolysis on sub-micron organic aerosols: the
623 effect of relative humidity, particle phase, and particle size, *Phys Chem Chem Phys*, 5, 4593-4603,
624 2003

625 van der A, R. J., Mijling, B., Ding, J., Koukouli, M. E., Liu, F., Li, Q., Mao, H., and Theys, N.: Cleaning
626 up the air: effectiveness of air quality policy for SO₂ and NO_x emissions in China, *Atmospheric
627 Chemistry and Physics*, 17, 1775-1789, 10.5194/acp-17-1775-2017, 2017.

628 Vayenas, D. V., Takahama, S., Davidson, C. I., and Pandis, S. N.: Simulation of the thermodynamics and
629 removal processes in the sulfate-ammonia-nitric acid system during winter: Implications for PM_{2.5}
630 control strategies, *J Geophys Res-Atmos*, 110, 2005.

631 Wang, D., Zhou, B., Fu, Q., Zhao, Q., Zhang, Q., Chen, J., Yang, X., Duan, Y., and Li, J.: Intense
632 secondary aerosol formation due to strong atmospheric photochemical reactions in summer:
633 observations at a rural site in eastern Yangtze River Delta of China, *The Science of the total
634 environment*, 571, 1454-1466, 10.1016/j.scitotenv.2016.06.212, 2016a.

635 Wang, H.L., Qiao, L.P., Lou S.R., Zhou, M., Ding, A.J., Huang, H.Y., Chen, J.M., Wang, Q., Tao, S.K.,
636 Chen, C.H., Li L., and Huang C.: Chemical composition of PM_{2.5} and meteorological impact among
637 three years in urban Shanghai, China, *Journal of Cleaner Production*, 112, 2, 1302-1311, 2016b.

638 Wang, H., Lu, K., Chen, X., Zhu, Q., Chen, Q., Guo, S., Jiang, M., Li, X., Shang, D., Tan, Z., Wu, Y.,
639 Wu, Z., Zou, Q., Zheng, Y., Zeng, L., Zhu, T., Hu, M., and Zhang, Y.: High N₂O₅ Concentrations
640 Observed in Urban Beijing: Implications of a Large Nitrate Formation Pathway, *Environmental
641 Science & Technology Letters*, 4, 416-420, 10.1021/acs.estlett.7b00341, 2017.

642 Wang, J., Ge, X., Chen, Y., Shen, Y., Zhang, Q., Sun, Y., Xu, J., Ge, S., Yu, H., and Chen, M.: Highly
643 time-resolved urban aerosol characteristics during springtime in Yangtze River Delta, China:
644 insights from soot particle aerosol mass spectrometry, *Atmospheric Chemistry and Physics*, 16,
645 9109-9127, 10.5194/acp-16-9109-2016, 2016c.

646 Wang, J., Zhao, B., Wang, S., Yang, F., Xing, J., Morawska, L., Ding, A., Kulmala, M., Kerminen, V.-M.,
647 Kujansuu, J., Wang, Z., Ding, D., Zhang, X., Wang, H., Tian, M., Petäjä, T., Jiang, J., Hao, J.,
648 Particulate matter pollution over China and the effects of control policies, *Science of the Total
649 Environment*, 584, 426-447, 2017a.

650 Wang, T., Nie, W., Gao, J., Xue, L. K., Gao, X. M., Wang, X. F., Qiu, J., Poon, C. N., Meinardi, S., Blake,
651 D., Wang, S. L., Ding, A. J., Chai, F. H., Zhang, Q. Z., and Wang, W. X.: Air quality during the 2008
652 Beijing Olympics: secondary pollutants and regional impact, *Atmospheric Chemistry and Physics*,
653 10, 7603-7615, 2010.

654 Wang, T., Tham, Y. J., Xue, L. K., Li, Q. Y., Zha, Q. Z., Wang, Z., Poon, S. C. N., Dube, W. P., Blake, D.
655 R., Louie, P. K. K., Luk, C. W. Y., Tsui, W., and Brown, S. S.: Observations of nitryl chloride and
656 modeling its source and effect on ozone in the planetary boundary layer of southern China, *J
657 Geophys Res-Atmos*, 121, 2476-2489, 10.1002/2015JD024556, 2016d.

658 Wang, X., and Zhang, Y.: Particulate Nitrate Formation in a Highly Polluted Urban Area: A Case Study
659 by Single-Particle Mass Spectrometry in Shanghai Environ. Sci. Technol, 43, 3061-3066, 2009.

660 Wang, X., Ding, X., Fu, X., He, Q., Wang, S., Bernard, F., Zhao, X., and Wu, D.: Aerosol scattering
661 coefficients and major chemical compositions of fine particles observed at a rural site in the central
662 Pearl River Delta, South China, Journal of Environmental Sciences, 24, 72-77, 10.1016/s1001-
663 0742(11)60730-4, 2012.

664 Wang, X. F., Chen, J. M., Sun, J. F., Li, W. J., Yang, L. X., Wen, L., Wang, W. X., Wang, X. M., Collett,
665 J. L., Shi, Y., Zhang, Q. Z., Hu, J. T., Yao, L., Zhu, Y. H., Sui, X., Sun, X. M., and Mellouki, A.:
666 Severe haze episodes and seriously polluted fog water in Ji'nan, China, Sci Total Environ, 493, 133-
667 137, 2014.

668 Wang, X., Wang, H., Xue, L., Wang, T., Wang, L., Gu, R., Wang, W., Tham, Y. J., Wang, Z., Yang, L.,
669 Chen, J., and Wang, W.: Observations of N₂O₅ and ClNO₂ at a polluted urban surface site in
670 North China: High N₂O₅ uptake coefficients and low ClNO₂ product yields, Atmospheric
671 Environment, 156, 125-134, 10.1016/j.atmosenv.2017.02.035, 2017b.

672 Wen, L., Chen, J., Yang, L., Wang, X., Caihong, X., Sui, X., Yao, L., Zhu, Y., Zhang, J., Zhu, T., and
673 Wang, W.: Enhanced formation of fine particulate nitrate at a rural site on the North China Plain in
674 summer: The important roles of ammonia and ozone, Atmospheric Environment, 101, 294-302,
675 10.1016/j.atmosenv.2014.11.037, 2015.

676 Wen, L., Xue, L., Wang, X., Xu, C., Chen, T., Yang, L., Wang, T., Zhang, Q., and Wang, W.: Summertime
677 fine particulate nitrate pollution in the North China Plain: increasing trends, formation mechanisms
678 and implications for control policy, Atmospheric Chemistry and Physics, 18, 11261-11275,
679 10.5194/acp-18-11261-2018, 2018.

680 Xie, Y., Ding, A., and Nie, W.: Enhanced sulfate formation by nitrogen dioxide: Implications from in situ
681 observations at the SORPES station Journal Of Geophysical Research: Atmospheres, 120, 12,679-
682 612,964, 10.1002/, 2015.

683 Xue., J., and Yuan., Z.: Insights into factors affecting nitrate in PM_{2.5} in a polluted high NO_x environment
684 through hourly observations and size distribution measurements Journal of Geophysical Research:
685 Atmospheres, 119, 4888-4902, 10.1002/, 2013.

686 Yang, T., Sun, Y., Zhang, W., Wang, Z., Liu, X., Fu, P., and Wang, X.: Evolutionary processes and sources
687 of high-nitrate haze episodes over Beijing, Spring, J Environ Sci (China), 54, 142-151,
688 10.1016/j.jes.2016.04.024, 2017.

689 Young, D. E., Kim, H., Parworth, C., Zhou, S., Zhang, X., Cappa, C. D., Seco, R., Kim, S., and Zhang,
690 Q.: Influences of emission sources and meteorology on aerosol chemistry in a polluted urban
691 environment: results from DISCOVER-AQ California, Atmospheric Chemistry and Physics, 16,
692 5427-5451, 10.5194/acp-16-5427-2016, 2016.

693 Zhang, Q., Canagaratna, M. R., Jayne, J. T., Worsnop, D. R., and Jimenez, J. L.: Time- and size-resolved
694 chemical composition of submicron particles in Pittsburgh: Implications for aerosol sources and

695 processes, *J Geophys Res-Atmos*, 110, 2005.

696 Zhang, Y., Tang, L., Yu, H., Wang, Z., Sun, Y., Qin, W., Chen, W., Chen, C., Ding, A., Wu, J., Ge, S.,
697 Chen, C., and Zhou, H.-c.: Chemical composition, sources and evolution processes of aerosol at an
698 urban site in Yangtze River Delta, China during wintertime, *Atmospheric Environment*, 123, 339-
699 349, 10.1016/j.atmosenv.2015.08.017, 2015a.

700 Zhang, Y. J., Tang, L. L., Wang, Z., Yu, H. X., Sun, Y. L., Liu, D., Qin, W., Canonaco, F., Prévôt, A. S.
701 H., Zhang, H. L., and Zhou, H. C.: Insights into characteristics, sources, and evolution of submicron
702 aerosols during harvest seasons in the Yangtze River delta region, China, *Atmospheric Chemistry
703 and Physics*, 15, 1331-1349, 10.5194/acp-15-1331-2015, 2015b.

704 Zhang, Y. W., Zhang, X. Y., Zhang, Y. M., Shen, X. J., Sun, J. Y., Ma, Q. L., Yu, X. M., Zhu, J. L., Zhang,
705 L., and Che, H. C.: Significant concentration changes of chemical components of PM1 in the
706 Yangtze River Delta area of China and the implications for the formation mechanism of heavy haze-
707 fog pollution, *The Science of the total environment*, 538, 7-15, 10.1016/j.scitotenv.2015.06.104,
708 2015c.

709 Zhang, Y., Ding, A., Mao, H., Nie, W., Zhou, D., Liu, L., Huang, X., and Fu, C.: Impact of synoptic
710 weather patterns and inter-decadal climate variability on air quality in the North China Plain during
711 1980-2013, *Atmos. Environ.*, 124, 119-128, 2016.

712 Zou, J., Liu, Z., Hu, B., Huang, X., Wen, T., Ji, D., Liu, J., Yang, Y., Yao, Q., and Wang, Y.: Aerosol
713 chemical compositions in the North China Plain and the impact on the visibility in Beijing and
714 Tianjin, *Atmospheric Research*, 201, 235-246, 10.1016/j.atmosres.2017.09.014, 2018.

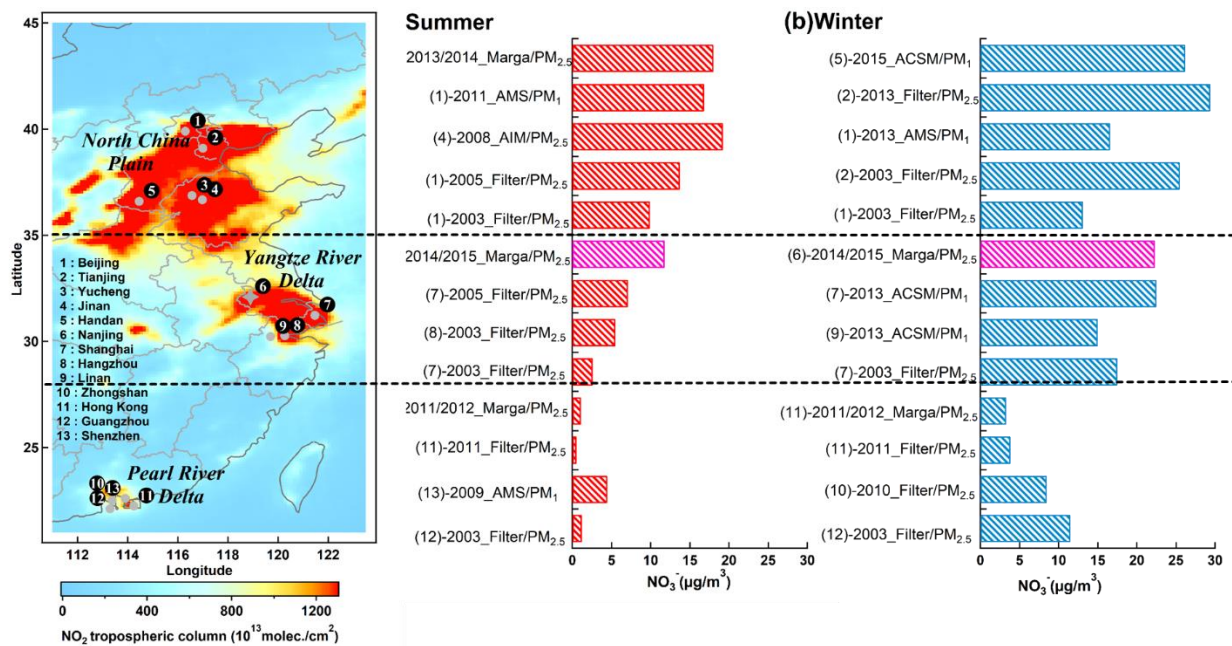


Figure 1 Average mass concentrations of particulate nitrate at different sampling sites in **(a)** summer and **(b)** winter. The left panel shows the map color-coded by 2-years (2014-2015) averaged tropospheric NO₂ from OMI satellite (<http://www.temis.nl/airpollution/no2.html>). The pink bars are for this study.

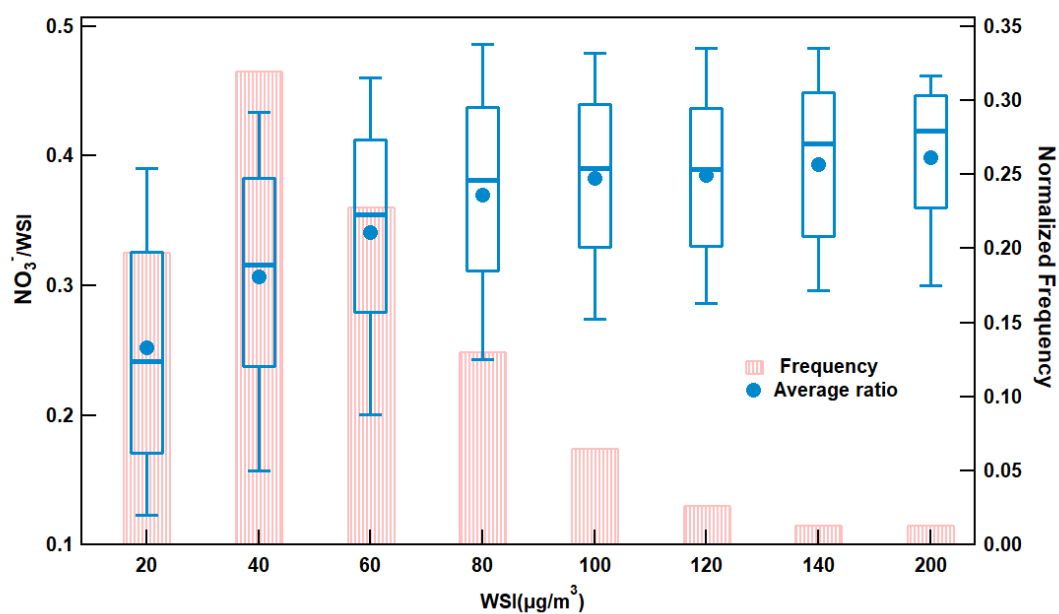


Figure 2 Average proportion of nitrate and normalized frequency of occurrence at different mass concentration bins of water soluble ions at SORPES. For the ratio, box boundaries represent the interquartile range, bars represent 5%-95% percentile range, and horizontal lines represent the median value.

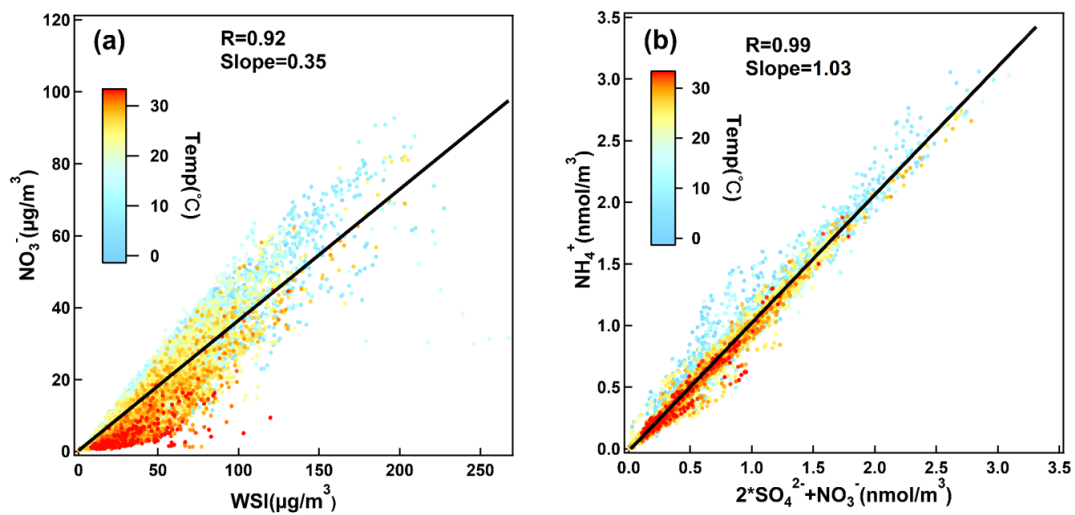


Figure 3 Scatter plots of (a) nitrate vs. total WSI color coded by air temperature, (b) molar concentrations of ammonium with nitrate molar concentrations plus two times of sulfate molar concentrations.

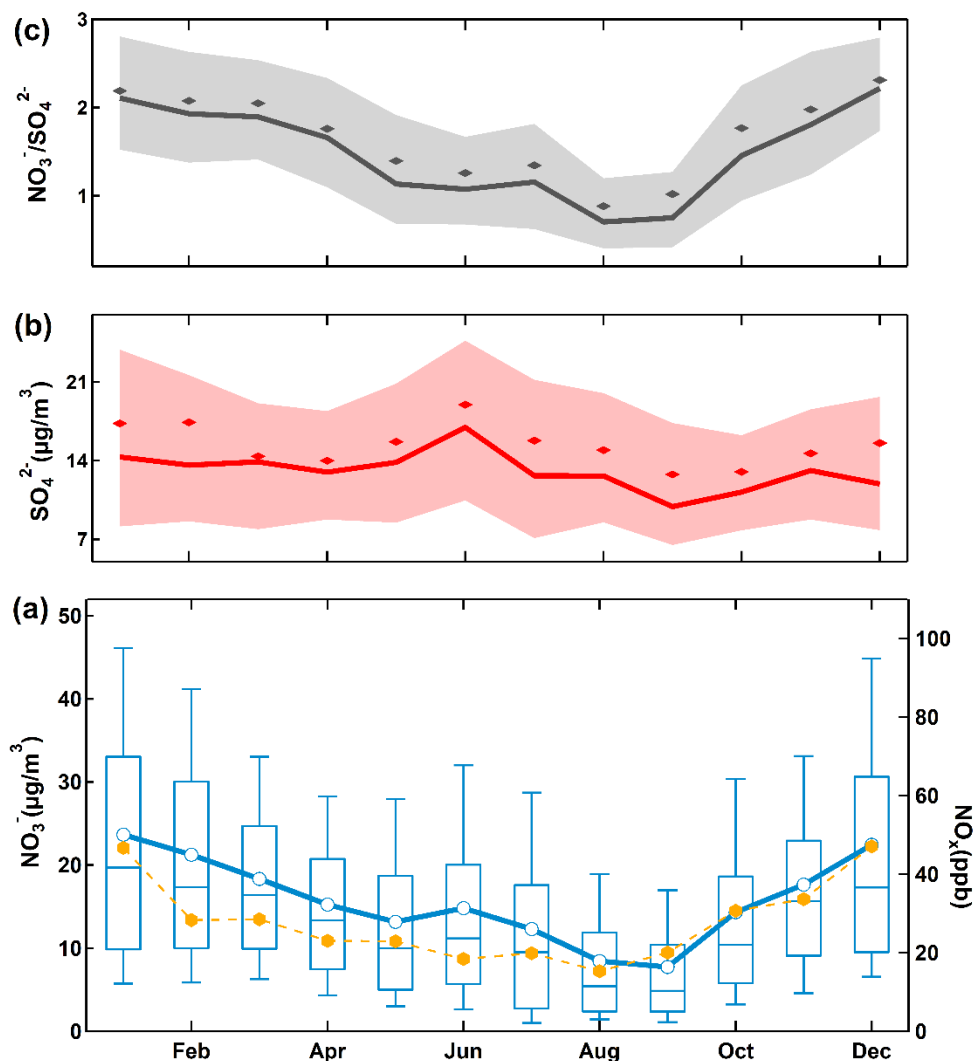


Figure 4 Monthly averaged nitrate (blue), sulfate (red), NO_x (orange) mass concentrations and nitrate to sulfate molar-based ratio (grey) measured at SORPES station during March 2014 to February 2016. For nitrate to sulfate ratio (a) and sulfate (b), bold solid lines are the median values, shade areas represent percentiles of 75% and 25%, and diamonds represent the mean values. For nitrate (c), box boundaries represent the interquartile range, bars represent 5%-95% percentile range, horizontal lines represent the median value, and crosses represent mean values.

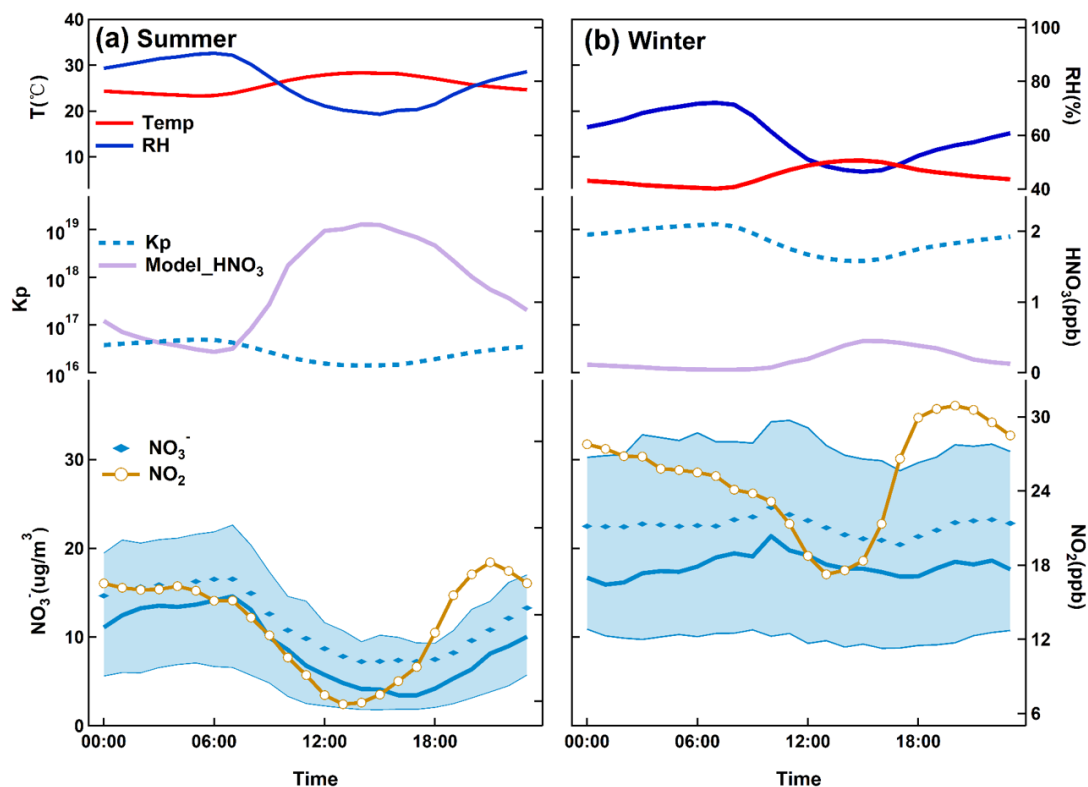


Figure 5 Diurnal variation of particulate nitrate in **(a)** summer and **(b)** winter. For nitrate, bold solid lines are the median values, shaded areas represent percentiles of 75% and 25% and diamonds represent mean values. Diurnal averages of NO_2 and modeled nitric acid concentrations are also provided with temperature and RH.

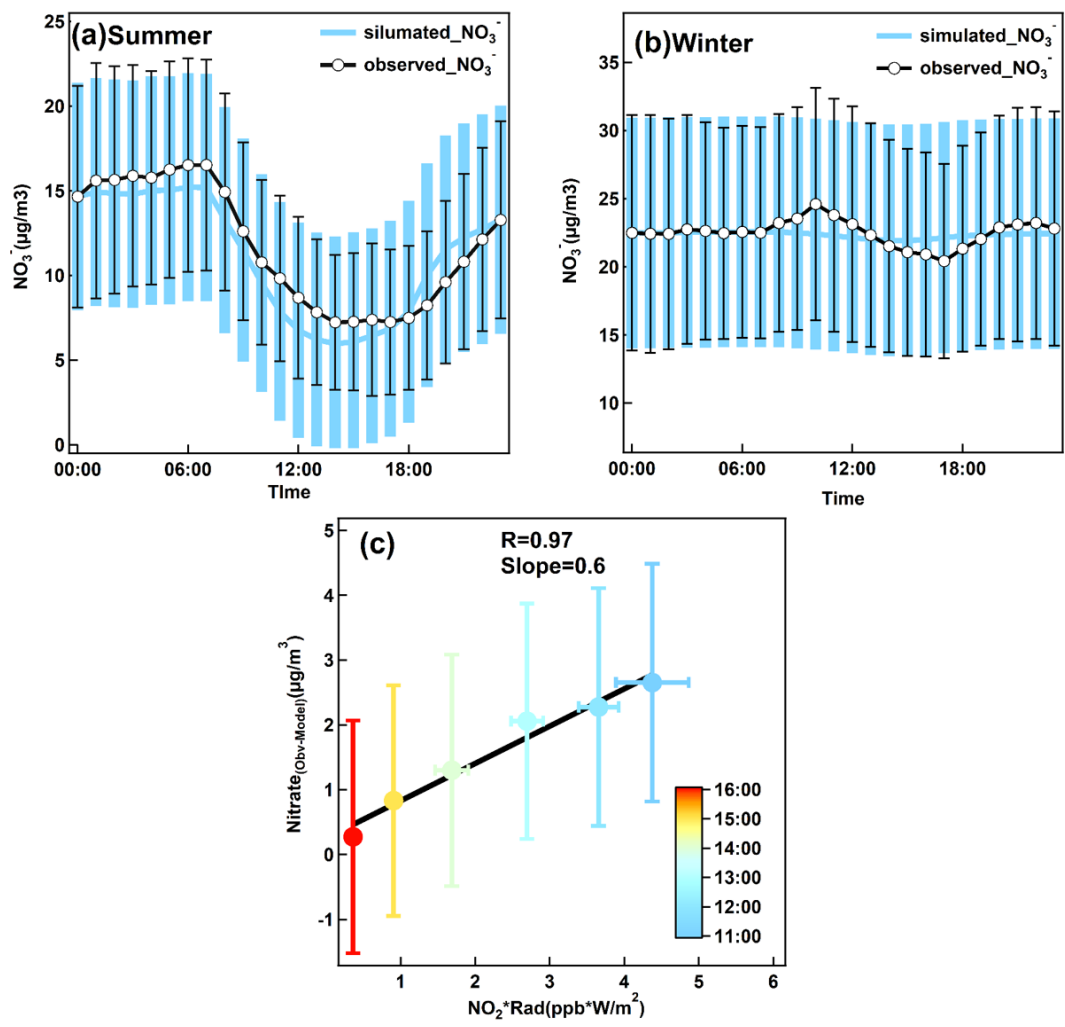


Figure 6 Modeled nitrate diurnal variations in **(a)** summer and **(b)** winter, together with the observed nitrate concentrations. Error bars provided are the standard deviation of the mean at each hourly interval. **(c)** Scatter plot of the difference between model and observed nitrate average mass concentrations with the product of NO_2 and radiation color coded by the hour of day for the samples.

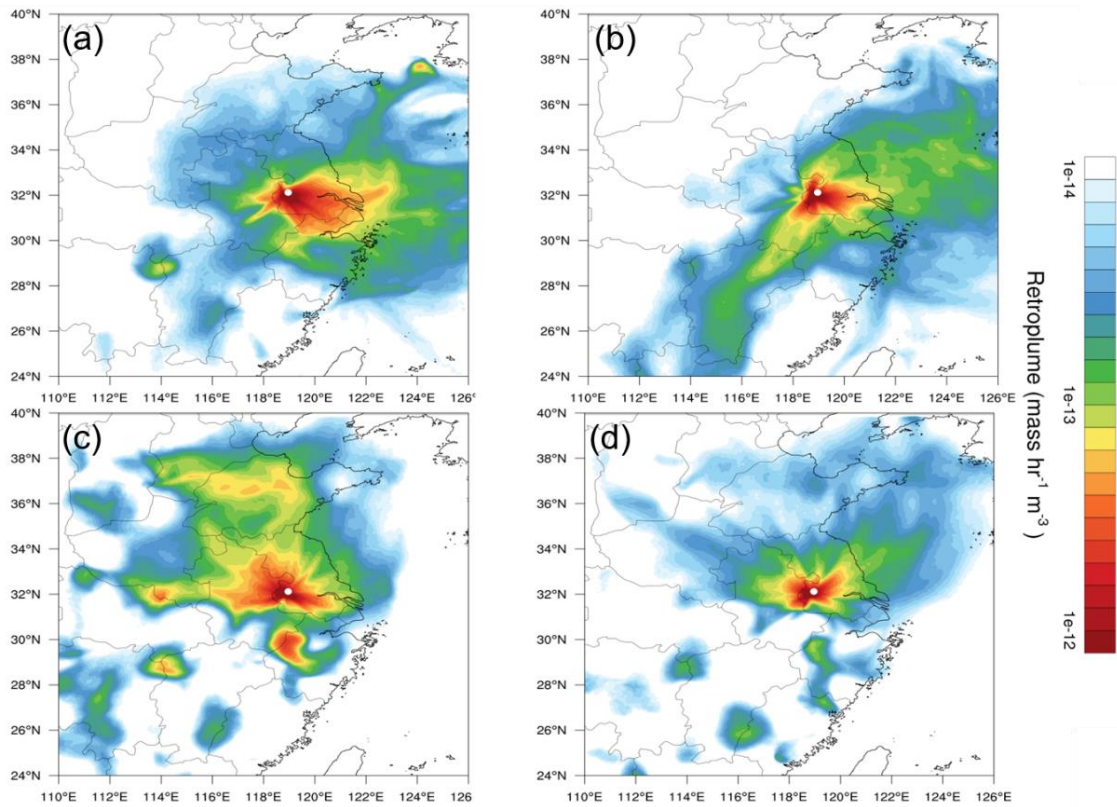


Figure 7 The averaged retroplumes (i.e., 100 m footprint) of the selected events: **(a)** Top 25% nitrate concentrations in summer, **(b)** Bottom 25% nitrate concentrations in summer, **(c)** Top 25% nitrate concentrations in winter, and **(d)** Bottom 25% nitrate concentrations in winter.

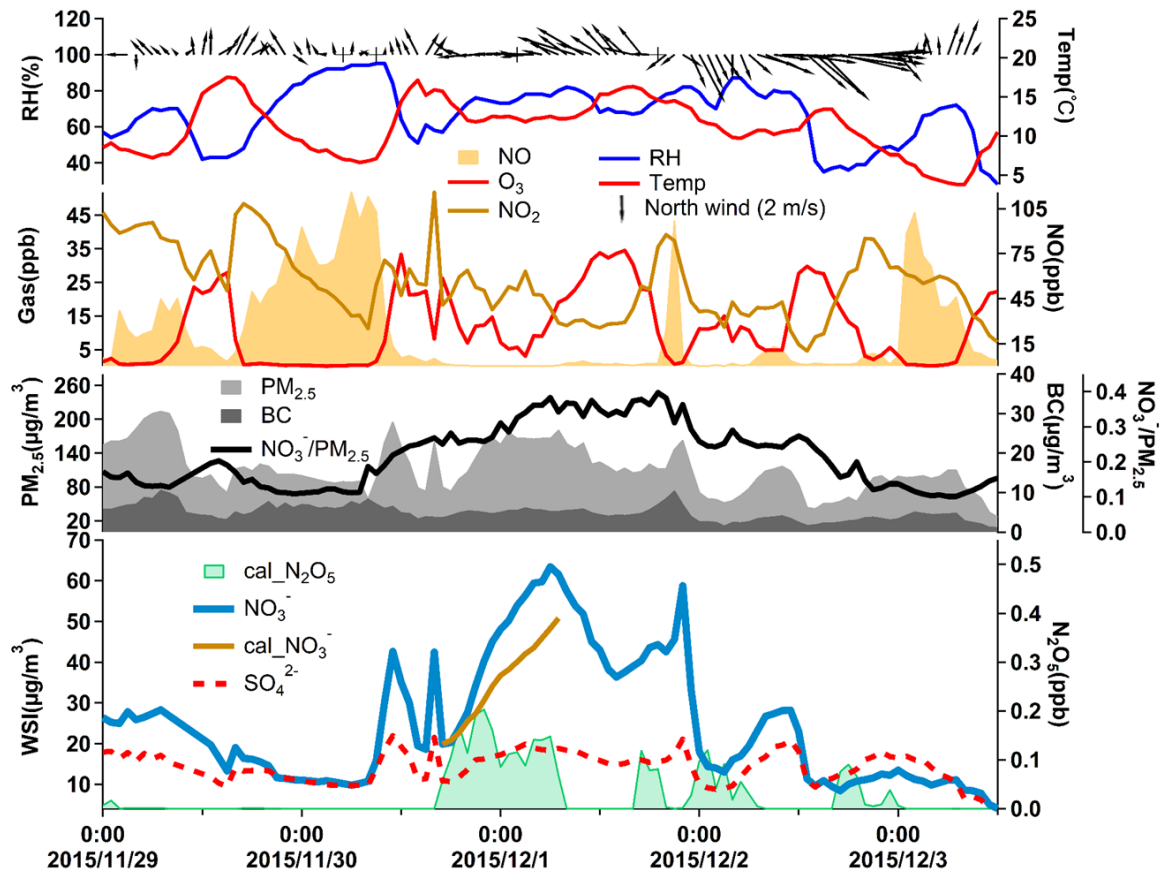


Figure 8 Time series of meteorological data and the concentrations of trace gases related to nitrate formation during 29 November to 3 December, 2015. Cal_NO₃⁻ represents the nitrate concentrations calculated from the hydrolysis of N₂O₅.

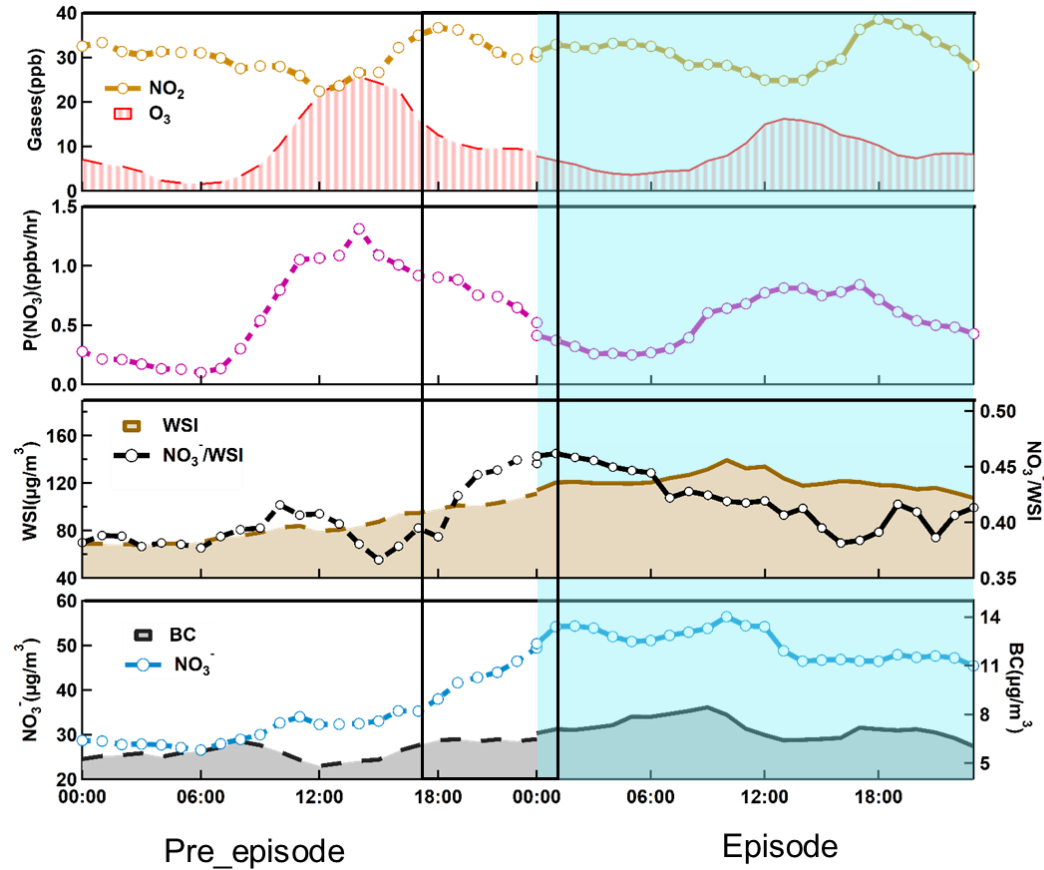


Figure 9 Diurnal variations of particulate nitrate, black carbon, the total water soluble ions, nitrate to WSI ratio, $P(\text{NO}_3)$, NO_2 , and O_3 averaged for nitrate episode days with exceedances of one mean plus two standard deviations. The left side shows the pre-episode days and the right side shows the episode days during the winter of entire two years period. The solid line box corresponds to the rapid growth of nitrate at night. It should be noted that $P(\text{NO}_3)$ is calculated by the product of NO_2 and O_3 multiplied by the rate constant k_1 of $\text{NO}_2 + \text{O}_3$ reaction.

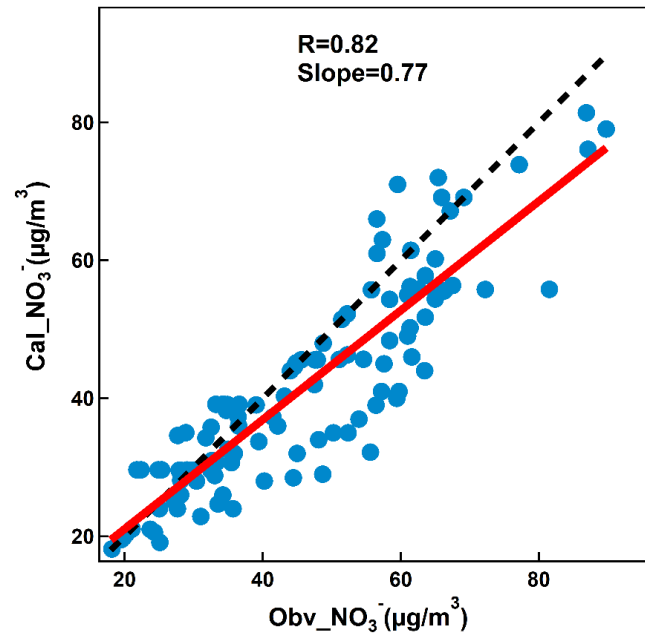


Figure 10 Scatter plot of calculated nitrate concentrations and observed nitrate concentrations from 17:00 to 23:00 of each episode.

Table 1 major gas phase and heterogeneous reactions involved NO₃ and N₂O₅

Reaction	Rate constant
$\text{NO}_2 + \text{O}_3 \rightarrow \text{NO}_3 + \text{O}_2$	$k_1 = 1.28 \times 10^{13} \times \text{EXP}(-2470/T)$
$\text{NO}_3 + \text{NO}_2 \leftrightarrow \text{N}_2\text{O}_5$	$k_{eq} = 1.73 \times 10^{-13} \times \text{EXP}(1550/T)$
$\text{NO}_3 + \text{NO} \leftrightarrow \text{NO}_2 + \text{NO}_2$	$k_3 = 1.8 \times 10^{-11} \times \text{EXP}(110/T)$
$\text{NO}_3 \rightarrow \text{NO} + \text{O}_2$	j_4
$\text{NO}_3 \rightarrow \text{NO} + \text{O}_2$	j_5
$\text{NO}_3 \xrightarrow{\text{voc}} \text{products}$	$k_6 = \sum (k_{\text{voci}} \cdot [\text{voc}]_i)$
$\text{NO}_3 \xrightarrow{\text{Heterogeneous}} \text{products}$	$k_7 = 0.25 \cdot i \cdot C_{\text{NO}_3} \cdot \gamma_{\text{NO}_3} \cdot S_{\text{aerosol}}$
$\text{N}_2\text{O}_5 \xrightarrow{\text{Heterogeneous}} \text{products}$	$k_8 = 0.25 \cdot C_{\text{N}_2\text{O}_5} \cdot \gamma_{\text{N}_2\text{O}_5} \cdot S_{\text{aerosol}}$